

Bridging the Evaluation Gap: Standardized Benchmarks for Multi-Objective Search

Hadar Peer¹, Carlos Hernandez², Sven Koenig³, Ariel Felner⁴, Oren Salzman¹

¹Technion – Israel Institute of Technology

²Universidad San Sebastián

³University of California, Irvine

⁴Ben-Gurion University

Abstract

Empirical evaluation in multi-objective search (MOS) has historically suffered from fragmentation, relying on heterogeneous problem instances with incompatible objective definitions that make cross-study comparisons difficult. This standardization gap is further exacerbated by the realization that DIMACS road networks, a historical default benchmark for the field, exhibit highly correlated objectives that fail to capture diverse Pareto-front structures. To address this, we introduce the first comprehensive, standardized benchmark suite for exact and approximate MOS. Our suite spans four structurally diverse domains: real-world road networks, structured synthetic graphs, game-based grid environments, and high-dimensional robotic motion-planning roadmaps. By providing fixed graph instances, standardized start-goal queries, and both exact and approximate reference Pareto-optimal solution sets, this suite captures a full spectrum of objective interactions: from strongly correlated to strictly independent. Ultimately, this benchmark provides a common foundation to ensure future MOS evaluations are robust, reproducible, and structurally comprehensive.

1 Introduction

Multi-objective shortest-path problems arise when a path between two locations must be optimized with respect to multiple, often conflicting objectives rather than a single objective. For example, minimizing path length may conflict with maximizing path safety, since shorter routes may pass closer to obstacles or hazardous regions. Instead of returning a single optimal path, these problems require computing a set of trade-off solutions known as the Pareto-optimal solution set. Such problems arise in domains where competing criteria must be balanced, including transporting hazardous materials (Bronfman et al. 2015), robotics (Fu et al. 2023), and more. The problem has been studied for decades, yet has recently received renewed attention as modern applications increasingly require reasoning about multiple competing objectives (Salzman et al. 2026). Over this period, substantial progress has been made in the design of exact and approximate multi-objective search (MOS) algorithms (Salzman et al. 2023).

Despite this algorithmic progress, empirical evaluation in MOS remains fragmented. Unfortunately, algorithmic evaluation has been inconsistent, making comparison of different works difficult, as each study often relies on a dif-

ferent set of benchmark instances (see, e.g., (Maristany de las Casas et al. 2023)). Algorithms are typically evaluated on problems drawn from different research communities, including road networks, synthetic graph generators and grid-based pathfinding environments (Demetrescu, Goldberg, and Johnson 2006; Funke, Laue, and Storandt 2017; Moghadam, Ebrahimi, and Harabor 2024; Weise and Mostaghim 2022). These instances often differ in objective definitions, query-generation procedures, and reporting protocols. As a result, comparisons across different works are often indirect, difficult to reproduce, and sensitive to instance-specific modeling choices.

Indeed, benchmark inconsistency has already been identified as a key challenge for the MOS community (Salzman et al. 2023). Moreover, DIMACS benchmarks, which are among the most commonly used datasets in MOS studies (e.g. (Ahmadi et al. 2024)), have recently been shown to exhibit highly correlated objectives (Halle et al. 2025), making them a questionable go to benchmark instance.

Because MOS evaluation is sensitive to instance properties (such as number of objectives, graph connectivity, edge-cost distributions, and inter-objective correlation, which influence the size and structure of the Pareto-front), a standard benchmark must systematically span the full spectrum of domain structures. To address this challenge, this paper takes a first step toward systematic standardization by introducing a benchmark suite that unifies diverse problem families under a consistent formulation and evaluation protocol. Our benchmark suite spans four benchmark families:

- F1 Road networks**, including classical DIMACS datasets and multi-objective routing instances;
- F2 Structured synthetic graphs**, enabling to control the numbers of objectives and inter-objective correlation;
- F3 Game-based grid environments**, derived from weighted 2D pathfinding maps; and
- F4 Robot motion-planning graphs**, constructed from sampling-based robot motion-planning algorithms.

For each family, we provide fixed graph instances, standardized start-goal query sets, and reference exact- and approximate Pareto-optimal solution sets (see Sec. 2 for formal definitions). All benchmarks use non-negative additive edge costs to ensure compatibility with classical MOS formulations.

Rather than replacing existing datasets, the suite both builds on existing benchmark families and introduces new benchmark families. Consequentially, this suite provides the missing coherent evaluation framework required for direct, reproducible comparisons of MOS algorithms. Full implementation details, generation scripts, query sets, and reference solution sets are provided in the repository¹, which also includes a step-by-step user guide for using the benchmark instances.

2 Notations and Problem Definition

We briefly formalize the exact and approximate multi-objective shortest-path (MOS) problems. A *MOS graph* is a tuple $G = (V, E, \mathbf{c})$, where V is a finite set of vertices, $E \subseteq V \times V$ is a finite set of edges, and $\mathbf{c} : E \rightarrow \mathbb{R}_{\geq 0}^d$ assigns a d -dimensional non-negative cost vector to each edge.

A path $\pi = v_1, \dots, v_n$ is a sequence of vertices such that $(v_i, v_{i+1}) \in E$. The *cost* of π is $\mathbf{c}(\pi) = \sum_{i=1}^{n-1} \mathbf{c}(v_i, v_{i+1})$.

For a minimization problem, a vector \mathbf{p} *dominates* \mathbf{q} (denoted $\mathbf{p} \preceq \mathbf{q}$) if $\mathbf{p}_i \leq \mathbf{q}_i$ for all i and $\mathbf{p}_j < \mathbf{q}_j$ for at least one j . Similarly, given an *approximation factor* $\varepsilon \in \mathbb{R}_{\geq 0}^d$, we say that \mathbf{p} ε -*dominates* \mathbf{q} if $\mathbf{p}_i \leq (1 + \varepsilon_i) \cdot \mathbf{q}_i$ for all i and $\mathbf{p}_j < (1 + \varepsilon_j) \cdot \mathbf{q}_j$ for at least one j .

Given start and goal vertices $v_s, v_g \in V$, a solution is any path from v_s to v_g . The Pareto-optimal solution set Π^* consists of all solutions π such that there exists no other solution π' with $\mathbf{c}(\pi') \preceq \mathbf{c}(\pi)$. Similarly, an ε -approximate Pareto set Π_ε^* is a set of solutions such that every solution in Π^* is ε -dominated by some solution in Π_ε^* .

Problem 1 (Exact MOS.) Given a MOS graph $G = (V, E, \mathbf{c})$ and vertices $v_s, v_g \in V$, compute the Pareto-optimal solution set Π^* .

Problem 2 (Approximate MOS.) Given a MOS graph $G = (V, E, \mathbf{c})$ and vertices $v_s, v_g \in V$, and ε , compute an ε -approximate Pareto set Π_ε^* .

Note. when $\varepsilon = 0$, Prob. 2 reduces to Prob. 1.

Objective correlation. To characterize the linear dependence between two objectives, we utilize the *Pearson correlation coefficient* (Casella and Berger 2021). For any two vectors X and Y , their Pearson correlation $\rho(X, Y) \in [-1, 1]$ quantifies the strength of their linear relationship, with 1, -1 , and 0 denoting strong positive, strong negative, and no linear correlation, respectively.

In our MOS setting, for a set of edges E recall that $c_i(e)$ denotes the cost of edge $e \in E$ under objective i . Following Halle et al. (2025), we evaluate the pairwise correlation between objectives i and j by computing the Pearson coefficient over their respective edge-cost vectors:

$$\rho_{i,j} := \rho(\mathbf{c}_i, \mathbf{c}_j),$$

where $\mathbf{c}_i = \langle c_i(e) \rangle_{e \in E}$. Throughout this work, we rely on $\rho_{i,j}$ (often simply denoted as ρ when i and j are clear from the context) to report and analyze the dependencies among objective edge costs.

¹<https://github.com/CRL-Technion/Multi-Objective-Search-Benchmarks>

3 Related Work

Exact and Approximate Search Algorithms. The landscape of multi-objective search (MOS) has matured significantly in recent years, encompassing a wide array of both exact and approximate methods. For comprehensive overviews of recent algorithmic progress and emerging applications, we refer the reader to recent surveys (Salzman et al. 2023, 2026). Historically rooted in multi-labeling approaches (Martins 1984), exact MOS has evolved to include highly efficient, specialized methods for the bi-objective setting, such as BOA* (Hernández et al. 2023), alongside general algorithmic paradigms like EMOA* (Ren et al. 2025). However, as exact Pareto fronts can grow exponentially with the number of objectives, the community has increasingly developed bounded-approximation techniques to ensure scalability. For instance, algorithms like A*pex (Zhang et al. 2022) utilize ε -dominance merging strategies to compute compact, approximate Pareto sets while preserving bounds on the quality of the Pareto set.

Extensions beyond the classical formulation. To maximize utility across the MOS community, our benchmark suite targets the “classical” formulation (see also Sec. 2): non-negative, additive edge-local costs evaluated via Pareto dominance. While recent algorithmic advancements have explored alternative extensions such as MOS with negative edge weights (Ahmadi et al. 2024), aggregation-based models (Peer et al. 2025), and hierarchical formulations (Slutsky et al. 2021), our benchmark suite focuses exclusively on the classical setting, leaving the standardization of these extended models for future work.

Benchmarking and evaluation practice. Empirical evaluation of heuristic MOS algorithms has historically relied on heterogeneous instance sources. Real-world road networks, particularly the DIMACS datasets (Demetrescu, Goldberg, and Johnson 2006), have been extensively used as a primary testbed due to their scale and practical relevance, while high-dimensional routing models (Funke, Laue, and Storandt 2017) have been explored to evaluate multi-objective transportation algorithms. Synthetic graph generators are similarly prevalent, enabling controlled analysis of objective dimensionality and interaction (Raith and Ehrgott 2009; Maristany de las Casas et al. 2023).

However, other prominent search domains lack equivalent standardized MOS datasets. Grid-based pathfinding and robotic motion planning rely on heavily standardized single-objective benchmarks such as the Moving AI repository (Sturtevant 2012), modern weighted grids like GUARDS (Moghadam, Ebrahimi, and Harabor 2024), and continuous motion planning suites (Moll, Şucan, and Kavraki 2015). Yet, standardized discrete MOS graphs for these environments are absent. Furthermore, while alternative many-objective pathfinding suites exist (Weise and Mostaghim 2022), they often incorporate history-dependent, non-additive costs that depart from the classical problem definition. Our benchmark suite addresses this disparity by unifying established road networks and synthetic generators with newly adapted, classical MOS instances derived from these single-objective grid and motion-planning domains.

Table 1: Summary of benchmark instances and exact Pareto set statistics ($\varepsilon = 0$). For grid benchmarks, statistics are aggregated over multiple grid instances of varying sizes. Median and mean Pareto cardinalities are rounded to the nearest integer.

Family	Benchmark	#Obj	Vertices	Edges	Min $ \Pi^* $	Max $ \Pi^* $	Median $ \Pi^* $	Mean $ \Pi^* $
F1	DIMACS-NY_2	2	264,346	733,846	3	808	94	157
	DIMACS-FLA_2	2	1,070,376	2,712,798	2	2,110	235	417
	DIMACS-Extended-NY_3	3	264,346	733,846	14	8,909	2,225	2,295
	DIMACS-Extended-NY_4	4	264,346	733,846	24	8,025	2,558	2,783
	DIMACS-Extended-NY_5	5	264,346	733,846	24	8,705	2,619	2,866
F2	GER_10	10	10,000	19,164	0	2,958	897	952
	Grid_2 $_{k \times m}$	2	$km + 2$	$\sim 4km$	135	540	238	270
	Grid_3 $_{k \times m}$	3	$km + 2$	$\sim 4km$	603	2,072	1,305	1,296
	Grid_4 $_{k \times m}$	4	$km + 2$	$\sim 4km$	568	2,853	1,653	1,661
	NetMaker-10k_3	3	10,000	59,943	36	1,343	253	326
	NetMaker-20k_3	3	20,000	119,909	67	1,276	369	424
	NetMaker-30k_3	3	30,000	179,739	101	1,423	418	485
F3	Games-FireWalker_2	2	196,608	1,138,856	0	225	63	73
	Games-64room_2	2	262,144	1,984,374	0	265	90	95
	Games-maze512_2	2	262,144	1,980,234	3	277	122	133
F4	Panda-RRG_2	2	20,000	364,770	2	258	51	65
	Panda-RRG_8	8	1,000	10,260	30	8,726	4,676	4,283

$$k, m \in \{300, 350, 400, 450, 500, 550, 600\}$$

4 The Benchmark Suite

In this section, we present our proposed benchmark suite for empirical evaluation in MOS. We first establish the design goals that guided its construction (Sec. 4.1). We then detail the four benchmark families that comprise the suite (road networks, synthetic graphs, game-based grids, and robot motion-planning roadmaps), specifying the objective definitions, structural topologies, and standardized query sets for each instance (Sec. 4.2–4.5). A summary of the scale (vertex and edge counts) and exact Pareto-front statistics for all benchmark instances is provided in Table 1.

Specifically, the suite builds on existing benchmark families, including road networks and structured synthetic graphs (Sec. 4.2, 4.3), and introduces new benchmark families, including game-based grid maps and robot motion-planning roadmaps (Sec. 4.4, 4.5).

All benchmark graphs are represented as directed graphs. When the underlying domain is undirected, edges are modeled bidirectionally.

4.1 Benchmark Design Goals

The benchmark suite is designed to support meaningful and reproducible empirical evaluation of MOS algorithms. Its construction is guided by the following goals.

- G1 Standardization.** Benchmarks are defined using fixed graph instances, objective formulations, and standardized start–goal query sets, enabling direct comparison across algorithms.
- G2 Reproducibility.** All benchmark components, including objective definitions, query sets, and reference solution sets, are fully documented and deterministic. We provide all source code and graph-generation scripts to allow re-

sults to be independently verified and to enable future users to generate additional benchmark instances.

- G3 Diversity.** The suite includes instances with varying numbers of objectives and objective interactions. These span qualitatively different graph topologies and cost-generation mechanisms, ranging from strongly correlated to nearly independent settings. As we will see, some benchmark families are designed to contain large Pareto fronts, while others include instances with disconnected components, requiring algorithms to efficiently determine that the start and goal are disconnected.
- G4 Compatibility.** When possible, our suite builds on existing graph datasets and established construction methodologies, even when alternative approaches are possible, to ensure consistency with prior work.
- G5 Extensibility.** The benchmark suite, alongside the provided generation scripts, is structured to facilitate the community-driven addition of new benchmark families, objectives, and query sets as MOS research evolves.

4.2 Road Networks

Road networks form a central benchmark family in MOS due to their practical relevance and widespread use in routing and transportation problems. While they are commonly used to evaluate routing metrics such as distance and travel time, these classical objective pairs often exhibit near-perfect correlation (i.e., $\rho \sim 1$), severely limiting the resulting trade-offs and Pareto-front cardinality (Halle et al. 2025). To address this and capture meaningful objective conflicts, the benchmark suite includes multiple datasets that extend beyond standard correlated pairs, varying in graph size, objective dimensionality, and objective definitions.

DIMACS Road Networks

Objectives. The DIMACS road-network benchmark defines two objectives: geographic distance and travel time. Both objectives are derived from the original DIMACS datasets and accumulated additively along paths, following the formulations used in the 9th DIMACS Implementation Challenge (Demetrescu, Goldberg, and Johnson 2006).

Structure. We include the New York (NY) and Florida (FLA) road networks.

Objective interaction. Distance and travel time are strongly positively correlated at the edge level, indicating substantial redundancy between the two classical objectives. Specifically, the Pearson correlation is $\rho = 0.96$ in NY and $\rho = 0.97$ in FLA.

Queries. Each instance provides 100 start–goal queries, sampled uniformly at random.

DIMACS–Extended Road Networks

Objectives. The DIMACS–Extended benchmark augments the NY road network with additional objectives: elevation difference between two adjacent vertices, average vertex degree of adjacent vertices, and hop count (unit edge cost), in addition to distance and travel time. Objective definitions follow the methodology introduced in the NWMOA* road-network benchmark (Ahmadi et al. 2024).

Structure. All variants are constructed on top of the NY graph, preserving its topology while extending dimensionality to three, four, or five objectives.

Objective interaction. While distance and travel time remain strongly correlated ($\rho \approx 0.96$), elevation exhibits only moderate correlation with them ($\rho = 0.38$ for both). Furthermore, average vertex degree and hop count exhibit negligible correlation with all other metrics (all $|\rho| < 0.08$), successfully introducing partially independent objective dimensions into the road network topology.

Queries. To enable direct performance comparisons against the base bi-objective setting, all extended variants evaluate on the same 100 fixed NY queries defined above.

GER10 Road Network

Objectives. The GER₁₀ benchmark defines ten edge-cost objectives following the high-dimensional routing objective definitions introduced in (Funke, Laue, and Storandt 2017), including distance, travel time, ascent, large roads, medium roads, small roads, gas price, energy, unit, and quietness. All objectives are represented as separate edge-cost functions and accumulated additively along paths.

Structure. The benchmark uses a connected subgraph of the original German road network. This subgraph is extracted via breadth-first search (BFS) to ensure connectivity. After extraction, vertices are remapped to contiguous identifiers while preserving spatial locality.

Objective interaction. GER₁₀ exhibits multiple highly correlated objective pairs. Several routing-related objectives (e.g., distance, energy consumption, gas price, and small-road preference) exhibit very strong positive correlation ($\rho > 0.95$). Additional pairs, including distance–travel time and road-type interactions, exhibit moderately strong correlation ($\rho \approx 0.8$).

Queries. Consistent with the other road-network instances, evaluation is standardized over a fixed set of 100 randomly sampled start–goal pairs.

4.3 Synthetic Graphs

Synthetic graph benchmarks provide a controlled environment for systematic experimentation. Their structure and cost assignments are generated programmatically, enabling precise control over graph topology, number of objectives, and objective interactions. In this suite, we include both independently generated grids and structured synthetic graph models (to be explained shortly).

Random-Cost Grids

Objectives. The Grid benchmark assigns either two, three, or four objective costs to grid edges. Each objective is generated independently by sampling integer costs uniformly at random from $[1, 10]$, following the methodology of Maristany de las Casas et al. (2023); Maristany de las Casas, Sedeño-Noda, and Borndörfer (2021).

Structure. The benchmark contains two-dimensional four-connected grid graphs constructed by independently selecting the width and height from $\{300, 350, 400, 450, 500, 550, 600\}$, yielding a total of $7 \times 7 = 49$ different graphs. These graphs are shared for each number of objectives (2, 3 and 4).

Each instance includes two auxiliary vertices defining a standardized source–target query: a source vertex connected to all vertices in the leftmost column and a target vertex receiving edges from all vertices in the rightmost column.

Objective interaction. Because the costs are sampled uniformly and independently, the objectives are nearly independent by construction. Across all variants, Pearson correlations satisfy $|\rho| < 0.01$.

Queries. Each instance defines a single source–target query between the auxiliary source and target vertices.

NetMaker

Objectives. NetMaker defines three non-negative, integer-valued objectives accumulated additively along paths, following structured synthetic constructions inspired by prior MOS benchmarks (Raith and Ehrgott 2009; Maristany de las Casas et al. 2023). Each edge e is assigned a cost vector $\mathbf{c}(e) \in \mathbb{Z}_{\geq 0}^3$.

Structure. Each instance is a directed graph $G = (V, E)$ with $V = \{1, \dots, N\}$ and $E = E_{\text{cyc}} \cup E_{\text{loc}}$. To define E_{cyc} , a uniformly random permutation $\sigma = (\sigma_1, \dots, \sigma_N)$ of V is sampled, and the directed Hamiltonian cycle

$$E_{\text{cyc}} = \{(\sigma_i, \sigma_{i+1}) \mid 1 \leq i < N\} \cup \{(\sigma_N, \sigma_1)\}$$

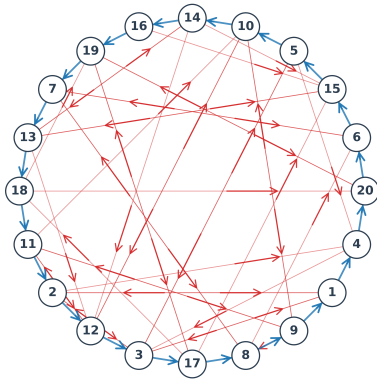


Figure 1: Illustration of the NetMaker graph construction for $|V| = 20$, $a_{\min} = 1$, $a_{\max} = 4$, and $I_{\text{vertex}} = 4$. Blue and red edges correspond to E_{cyc} and E_{loc} , respectively. Vertices are arranged according to the Hamiltonian cycle for visualization; since locality is defined in vertex-ID space rather than cycle order, some locality edges appear to connect distant vertices in the drawing.

is added. This guarantees that every vertex lies on a directed cycle connecting all vertices, ensuring strong connectivity.

The additional edge set E_{loc} controls graph density by adding additional edges in the neighborhood of each vertex.

Specifically, to define *number* of additional edges, let a_{\min} and a_{\max} denote parameters controlling the minimum and maximum out-degree of a vertex. Now, for each vertex $u \in V$, a target out-degree is sampled uniformly from $\{a_{\min} + 1, \dots, a_{\max}\}$ (here, the extra 1 accounts for the outgoing cycle edge already present in E_{cyc}).

To define the *neighborhood* edges in E_{loc} span, let $I_{\text{vertex}} \in \mathbb{Z}^+$ denote a locality parameter controlling the size of the vertex-ID window used when generating edges in E_{loc} . This constraint restricts edges to connect vertices that are nearby in vertex-ID space, creating locally clustered graph structure while preserving global connectivity through the Hamiltonian backbone. Varying I_{vertex} controls the effective “shortcut” length in the graph, producing instances with different routing difficulty and Pareto-front structure. The locality window for vertex u is defined as

$$W(u) = \left[\max \left(1, u - \lfloor \frac{I_{\text{vertex}}}{2} \rfloor \right), \min \left(N, u + \lfloor \frac{I_{\text{vertex}}}{2} \rfloor \right) \right],$$

excluding self-loops, duplicate edges, and edges already in E_{cyc} , until the sampled out-degree is reached or no valid local edge remains. Importantly, locality is defined in vertex-ID space rather than along the Hamiltonian cycle, so vertices that are close in ID may be far apart in cycle order.

Costs depend on edge type. For each cycle edge $e \in E_{\text{cyc}}$, exactly one objective value is sampled from each of the intervals $[1, 333]$, $[334, 666]$, and $[667, 1000]$, with the assignment of intervals to objectives randomly permuted independently per edge. For each additional edge $e \in E_{\text{loc}}$, all three objective values are sampled independently and uniformly from $[1, 99]$. This makes shortcut edges significantly cheaper than cycle edges, creating alternative routing options while the Hamiltonian backbone determines the overall path length scale.

The current release contains 12 graphs: three size groups ($N \in \{10,000, 20,000, 30,000\}$), two locality settings ($I_{\text{vertex}} \in \{20, 50\}$), and two graphs per configuration. All instances use $a_{\min} = 1$ and $a_{\max} = 10$, yielding average out-degree close to 6. Table 1 reports the average edge counts for the three size groups. Figure 1 illustrates the construction on a small example.

Objective interaction. Objective interaction differs by edge type. On Hamiltonian-cycle edges (E_{cyc}), each edge receives one low, medium, and high magnitude cost component, randomly assigned to the three objectives. This induces moderate negative correlation between objective pairs ($\rho \approx -0.44$ on average). In contrast, additional locality edges (E_{loc}) are assigned independent uniform costs in $[1, 99]$ and therefore exhibit negligible correlation ($\rho \approx 0$).

Queries. Each graph is paired with 50 randomly sampled start-goal queries. Source vertices are sampled from the first 10% of vertex identifiers and target vertices from the last 10%. Because additional edges are restricted by the locality parameter I_{vertex} , most paths must traverse multiple intermediate regions of the graph rather than using direct long-range shortcuts. This encourages long-range routing tasks with many alternative paths, resulting in large Pareto fronts. Note, this construction is designed to reduce the occurrence of trivial or very small Pareto fronts, instead promoting queries with rich trade-offs and larger Pareto sets. Other benchmark families in the suite capture a broader range of Pareto-front sizes.

4.4 Game-Based Grid Environments

Game-based grid benchmarks are derived from weighted pathfinding maps originally designed for single-objective evaluation in video-game environments. These maps exhibit diverse geometric layouts, including open regions, mazes, and room-based layouts.

In this family, maps are converted into bi-objective shortest path instances capturing geometric path length and guard exposure (defined as the number of guards that have line-of-sight to a given cell). The resulting graphs are large, 8-connected grids, and exhibit weak correlation between objectives. These benchmarks complement both road networks and synthetic grids by introducing real-world-style spatial layouts with structurally independent objective components.

GUARDS-Based Grid Benchmarks

Objectives. The Games benchmark defines two objectives on grid maps derived from the GUARDS weighted pathfinding benchmark (Moghadam, Ebrahimi, and Harbor 2024). While the original GUARDS benchmark was designed for single-objective weighted pathfinding, we convert each map into a bi-objective shortest path formulation capturing path length and guard exposure.

The first objective captures path length, where orthogonal moves incur a cost of 10 and diagonal moves incur a cost of 14, approximating Euclidean distances.

The second objective captures “guard exposure” which models the number of guards observing a region and provides a spatially structured risk measure. This objective is

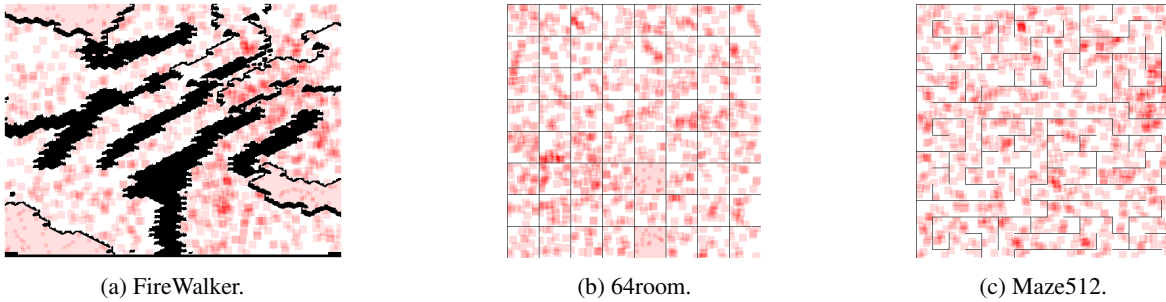


Figure 2: `Games` benchmark environments. Black regions denote obstacles. Red intensity reflects cost magnitude with darker red indicating regions observed by multiple guards.

new in the context of MOS benchmarking. For each vertex, the exposure is defined as the maximum number of guards observing the cell (i.e., having a line-of-sight to that cell). For orthogonal moves, the exposure cost equals the guard value of the destination cell. For diagonal moves, exposure equals the maximum guard value among the destination cell and the two intermediate side cells crossed by the diagonal. Diagonal moves are allowed only when both side cells are passable.

Structure. Each map is converted into a directed eight-connected graph, where each valid move becomes a directed edge. The current release includes three large-scale maps derived from the `GUARDS` benchmark (Moghadam, Ebrahimi, and Harabor 2024), see Fig 2. Grid sizes range between approximately 200,000 and 260,000 vertices with over one million directed edges per instance.

Objective interaction. For all instances, the Pearson correlation between objectives is small (in all cases, $|\rho| < 0.07$), indicating near-independence between objectives.

Queries. For each map, 100 start–goal queries are defined. Queries are sampled uniformly from passable cells with some sampled queries corresponding to disconnected source–target pairs; such cases are retained and result in empty solution sets.

4.5 Robot Motion-Planning Roadmaps

Robot motion-graph benchmarks are derived from sampling-based manipulation planning problems. In this family, roadmap graphs are constructed for the Franka Emika Panda 7-DoF arm in a fixed tabletop manipulation scene (Fig 4a). Each roadmap induces a MOS instance, enabling evaluation on realistic high-dimensional planning graphs with objectives that trade off motion efficiency and obstacle clearance.

Panda Motion-Planning Roadmaps

Objectives. The `Panda` benchmark defines multi-objective shortest path instances on Franka Emika Panda motion-planning roadmap graphs. Each edge (u, v) corresponds to a collision-free linear interpolation between joint configurations q_u and q_v . Subsequent objectives capture obstacle clearance, measured as the minimum Euclidean

workspace distance d along the edge. The benchmark supports both aggregated and per-link clearance formulations (detailed shortly). While aggregated clearance yields a standard bi-objective trade-off between path length and safety, the per-link formulation exposes structured many-objective trade-offs across individual robot links (Fig 4b).

Specifically, the first objective captures joint-space path length:

$$c_1(u, v) = \|q_u - q_v\|_2.$$

To define the clearance objectives, recall that clearance is measured as the geometric minimum distances between robot links and obstacles along an edge. Inspired by trajectory optimization in motion planning (e.g., `CHOMP` (Ratliff et al. 2009) and `STOMP` (Kalakrishnan et al. 2011)), clearance is converted into an additive cost objective via a smooth, penalty function that penalizes proximity within a safety margin δ which increases smoothly as the robot approaches obstacles while remaining zero beyond a safety margin. Set

$$U(d) = \begin{cases} 0 & \text{if } d \geq \delta, \\ \frac{1}{2\delta}(d - \delta)^2 & \text{if } 0 < d < \delta, \end{cases}$$

where d denotes the distance to the nearest obstacle and δ defines the clearance safety band. We will use $U(d)$ to define both bi- and multi-objective formulations.

Bi-objective formulation. Clearance is aggregated across all seven arm links:

$$c_2(u, v) = U(d_{\min}(u, v)),$$

where $d_{\min}(u, v)$ is the minimum clearance over all links along the edge. This yields a two-objective problem (path length and aggregated clearance) named `Panda-RRG_2`.

Many-objective formulation. Clearance is defined separately for each of the seven arm links. Let $d_i(u, v)$ denote the minimum clearance of link i along the edge. For the many-objective instance, components c_2, \dots, c_8 correspond to per-link clearance penalties:

$$c_i(u, v) = U(d_{i-1}(u, v)), \quad i = 2, \dots, 8.$$

This yields an eight-objectives problem named `Panda-RRG_8` (joint-space path length and seven per-link clearance objectives). Importantly, the two links closest to the base remain consistently far from obstacles, resulting in zero clearance penalties across all edges. We

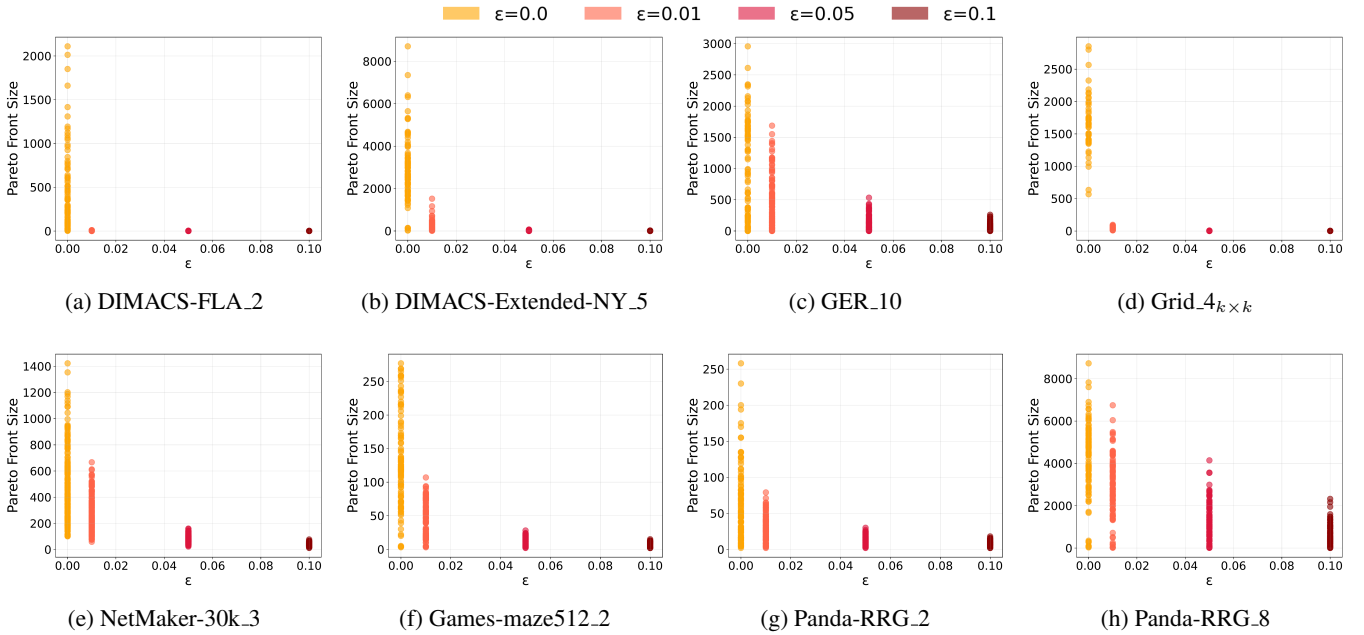


Figure 3: Pareto-front cardinality across queries as a function of the approximation parameter ε for representative benchmarks from all benchmark families. Each point corresponds to a start–goal query.

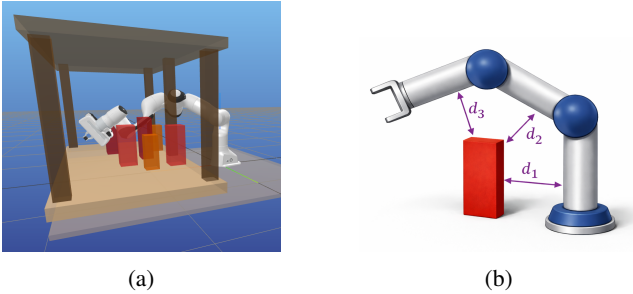


Figure 4: (a) Panda RRG benchmark environment of a Franka Emika Panda manipulator a tabletop scene featuring vertical support pillars, and box-shaped obstacles. (b) Illustration of link-specific clearance distances (d_1 , d_2 , d_3) in a 2D setting. Unlike an aggregated clearance model which collapses safety into a single minimum-distance penalty (here, d_2), a per-link formulation preserves the geometric risk profile across the entire manipulator.

retain these objectives to preserve structural consistency across instances and to reflect the true geometric structure of the manipulator, even when certain links are weakly constrained in a particular scene.

Structure. Roadmaps are generated using a Rapidly-exploring Random Graph (RRG) (Karaman and Frazzoli 2011), with a fixed connection radius of 1.5 radians in joint space. The clearance safety band parameter is set to $\delta = 0.1$ m. The current release includes two roadmap instances: Panda-RRG_2 and Panda-RRG_8.

Objective interaction. Pearson correlations are computed over all edges in each roadmap. For the bi-objective in-

stance, the correlation between path length and aggregated clearance is $\rho = 0.38$, indicating moderate positive correlation. For the many-objective instance, most of the 28 objective pairs exhibit weak correlation ($|\rho| < 0.3$); the largest observed correlations are 0.56 (between c_5 and c_6) and 0.43 (between c_4 and c_5).

Queries. For each instance, 100 randomly sampled and fixed start–goal queries are defined.

5 Standardized Evaluation Protocol

Evaluation is performed over the fixed start–goal query sets provided for each benchmark. Exact evaluation corresponds to computing the complete Pareto-optimal solution set for each query. Approximate evaluation follows an ε -dominance framework, using $\varepsilon \in \{0.0, 0.01, 0.05, 0.1\}$. Each query is evaluated independently for every ε value.

For approximate evaluation, the ordering of objectives affects the resulting solution sets. To ensure reproducibility, the objective ordering used for each benchmark and variant is fixed and explicitly documented in the repository.

Reference solution sets are computed using the NAMOA*dr algorithm as implemented in the A*pex codebase². NAMOA*dr is a MOS algorithm capable of enumerating exact Pareto-optimal solution sets as well as ε -approximate solution sets under ε -dominance (under mild algorithmic modifications (Zhang et al. 2022)).

All reference solution sets provided in the repository are generated using fixed objective definitions, objective orderings (for approximate cases), and ε values.

²<https://github.com/HanZhang39/A-pex>.

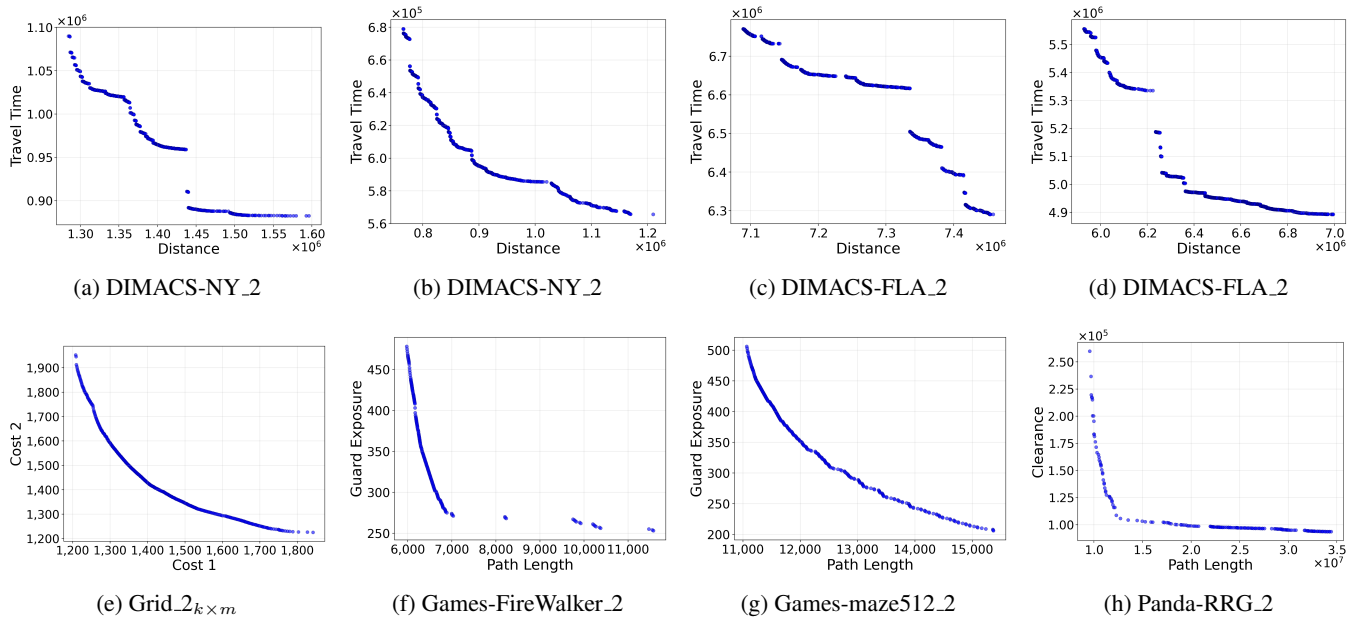


Figure 5: Representative exact two-objective Pareto fronts for single queries from different benchmark families. The examples highlight substantial variation in objective-space geometry across the benchmark suite.

Benchmark	Avg. Spread _x	Avg. Spread _y
DIMACS-NY_2	1.40	1.14
DIMACS-FLA_2	1.22	1.06
Grid_2 $k \times m$	1.63	3.24
Games-FireWalker_2	1.45	2.68
Games-maze512_2	1.22	2.15
Panda-RRG_2	2.35	3.17

Table 2: Spread (max/min ratio) of Pareto solutions along each objective axis for the representative instances (average over all queries) shown in Fig. 5. Larger values indicate greater variation along that objective.

6 Reference Solution Properties

To summarize exact Pareto-optimal solution sets, we report the median and mean Pareto cardinality per query for $\varepsilon = 0$. Table 1 presents benchmark scale and exact Pareto set statistics. For grid benchmarks, vertex and edge counts vary across instances and are reported as ranges.

Across a selected benchmarks of all benchmark families, Pareto set cardinality decreases substantially as ε increases, see Fig 3. Averaged over benchmark families, the median Pareto set size at $\varepsilon = 0.1$ is reduced by 97.9% relative to the exact case (95.6% mean reduction), with reductions ranging from 84.2% to 99.9% across benchmarks. Reference solution sets for all ε values are provided in the repository.

The representative Pareto fronts in Fig. 5 illustrate the diversity of objective-space structures across the benchmark families. For visualization, we focus on two-objective instances, which can be directly plotted in two-dimensional objective space. Table 2 reports the spread of Pareto solutions along each objective axis for these instances. Overall, the examples suggest that benchmark families differ not only

in Pareto-front size but also in the geometry and distribution of their solution sets.

7 Conclusion and Future Work

For years, the MOS community struggled with fragmented empirical evaluation, relying on heterogeneous problem instances that make cross-algorithmic comparisons difficult. This standardization gap has recently been exacerbated by the realization that the DIMACS road networks, a default benchmark for the field, exhibit highly correlated objectives. Relying on such narrow objective interactions severely limits our ability to evaluate how algorithms handle diverse, conflicting Pareto-front structures.

In this paper, we bridge this gap by introducing the first standardized benchmark suite for exact and approximate MOS. By unifying four structurally diverse domains, we provide a common foundation for empirical evaluation. Our suite offers fixed instances, standardized query sets, and reference Pareto-optimal solutions that span the spectrum from strongly correlated to entirely independent objectives.

While this initial release focuses on classical non-negative additive edge-local costs, the suite is designed to be extensible. Future work will expand the benchmark to encompass emerging extensions in the field, including aggregation-based models, hierarchical formulations, and history-dependent objectives. By providing this unified framework, we aim to accelerate algorithmic development and ensure that future MOS evaluations are robust, reproducible, and structurally comprehensive.

References

Ahmadi, S.; Sturtevant, N. R.; Harabor, D.; and Jalili, M. 2024. Exact Multi-objective Path Finding with Negative

- Weights. In *ICAPS*, 11–19.
- Bronfman, A.; Marianov, V.; Paredes-Belmar, G.; and Lier-Villagra, A. 2015. The maximin HAZMAT routing problem. *Eur. J. Oper. Res.*, 241(1): 15–27.
- Casella, G.; and Berger, R. L. 2021. *Statistical Inference*. Cengage Learning.
- Demetrescu, C.; Goldberg, A. V.; and Johnson, D. S. 2006. 9th DIMACS Implementation Challenge: Shortest Paths. <https://www.dis.uniroma1.it/~challenge9/>.
- Fu, M.; Kuntz, A.; Salzman, O.; and Alterovitz, R. 2023. Asymptotically optimal inspection planning via efficient near-optimal search on sampled roadmaps. *Int. J. of Rob. Res.*, 42(4-5): 150–175.
- Funke, S.; Laue, S.; and Storandt, S. 2017. Personal Routes with High-Dimensional Costs and Dynamic Approximation Guarantees. In *SEA*, volume 75, 18:1–18:13.
- Halle, Y.; Felner, A.; Koenig, S.; and Salzman, O. 2025. A Preprocessing Framework for Efficient Approximate Bi-Objective Shortest-Path Computation in the Presence of Correlated Objectives. In *SoCS*, volume 18.
- Hernández, C.; Yeoh, W.; Baier, J. A.; Zhang, H.; Suazo, L.; Koenig, S.; and Salzman, O. 2023. Simple and efficient bi-objective search algorithms via fast dominance checks. *Artif. Intell.*, 314: 103807.
- Kalakrishnan, M.; Chitta, S.; Theodorou, E.; Pastor, P.; and Schaal, S. 2011. STOMP: Stochastic Trajectory Optimization for Motion Planning. In *ICRA*, 4569–4574.
- Karaman, S.; and Frazzoli, E. 2011. Sampling-based Algorithms for Optimal Motion Planning. *Int. J. of Rob. Res.*, 30(7): 846–894.
- Maristany de las Casas, P.; Kraus, L.; Sedeño-Noda, A.; and Borndörfer, R. 2023. Targeted Multiobjective Dijkstra Algorithm. *Networks*, 82(3): 277–298.
- Maristany de las Casas, P.; Sedeño-Noda, A.; and Borndörfer, R. 2021. An Improved Multiobjective Shortest Path Algorithm. *Comp. & OR*, 135: 105424.
- Martins, E. Q. V. 1984. On a multicriteria shortest path problem. *Eur. J. Oper. Res.*, 16(2): 236–245.
- Moghadam, S. K.; Ebrahimi, M.; and Harabor, D. D. 2024. Guards: Benchmarks for weighted grid-based pathfinding. *Expert Syst. Appl.*, 249: 123719.
- Moll, M.; Şucan, I. A.; and Kavraki, L. E. 2015. Benchmarking Motion Planning Algorithms: An Extensible Infrastructure for Analysis and Visualization. *IEEE Robot. Autom. Mag.*, 22(3): 96–102.
- Peer, H.; Weiss, E.; Alterovitz, R.; and Salzman, O. 2025. Generalizing Multi-Objective Search via Objective-Aggregation Functions. arXiv:2509.22085.
- Raith, A.; and Ehrgott, M. 2009. A comparison of solution strategies for biobjective shortest path problems. *Comp. & OR*, 36(4): 1299–1331.
- Ratliff, N.; Zucker, M.; Bagnell, J. A.; and Srinivasa, S. 2009. CHOMP: Gradient Optimization Techniques for Efficient Motion Planning. In *ICRA*, 489–494.
- Ren, Z.; Hernández, C.; Likhachev, M.; Felner, A.; Koenig, S.; Salzman, O.; Rathinam, S.; and Choset, H. 2025. EMOA*: A framework for search-based multi-objective path planning. *Artif. Intell.*, 339: 104260.
- Salzman, O.; Felner, A.; Hernández, C.; Zhang, H.; Chan, S.; and Koenig, S. 2023. Heuristic-Search Approaches for the Multi-Objective Shortest-Path Problem: Progress and Research Opportunities. In *IJCAI*, 6759–6768.
- Salzman, O.; Ulloa, C. H.; Felner, A.; and Koenig, S. 2026. Multi-Objective Search: Algorithms, Applications, and Emerging Directions. In *AAAI*, 40990–40999.
- Slutsky, K.; Yershov, D.; Wongpiromsarn, T.; and Frazzoli, E. 2021. Hierarchical Multiobjective Shortest Path Problems. In *WAFR*, 261–276. Springer.
- Sturtevant, N. R. 2012. Benchmarks for grid-based pathfinding. *IEEE Trans. Comput. Intell. AI Games*, 4(2): 144–148.
- Weise, J.; and Mostaghim, S. 2022. A Scalable Many-Objective Pathfinding Benchmark Suite. *IEEE Trans. Evol. Comput.*, 26(1): 188–194.
- Zhang, H.; Salzman, O.; Kumar, T. K. S.; Felner, A.; Ulloa, C. H.; and Koenig, S. 2022. A*pex: Efficient Approximate Multi-Objective Search on Graphs. In *ICAPS*, 394–403.